

We are IntechOpen, the world's leading publisher of Open Access books Built by scientists, for scientists

6,900

Open access books available

186,000

International authors and editors

200M

Downloads

Our authors are among the

154

Countries delivered to

TOP 1%

most cited scientists

12.2%

Contributors from top 500 universities



WEB OF SCIENCE™

Selection of our books indexed in the Book Citation Index
in Web of Science™ Core Collection (BKCI)

Interested in publishing with us?
Contact book.department@intechopen.com

Numbers displayed above are based on latest data collected.
For more information visit www.intechopen.com



Neutron Diffraction on Acoustic Waves in a Perfect and Deformed Single Crystals

E. Raitman, V. Gavrilov and Ju. Ekmanis

Additional information is available at the end of the chapter

<http://dx.doi.org/10.5772/55064>

1. Introduction

The effect of crystal vibrations on the scattering of neutrons and X-rays in single crystals has already been studied for several decades. Crystals subjected to ultrasonic excitations have been investigated for some time by X-ray and neutron diffraction methods. The first X-ray diffraction experiments on oscillating crystals were performed in 1931 [1,2] stimulating large discussion to explain the observed increase in intensity of the Laue spots. Neutron experiments go back to the 60's [3-5]. At present time both neutrons and X-rays have become important tools in observing and understanding time-dependent matter-wave optics [6-8]. And vice versa the studying of the neutron and X-rays scattering in the time- and space-modulated with acoustic waves condensed matter represents a great interest. Applications from focusing effects [9], monochromators with tunable bandwidths [10-12], the characterization of static but tiny strain fields [13,14] have been discussed as well as fundamental questions about the formation of satellites [8] and its applications, inter-branch scattering, gradient crystal effects and the fundamental difference between neutron- and X-ray diffraction found their audience [15,16]. Theoreticians have tried to explain the variety of effects and have predicted even more challenging fields for experimentalists, like, for example, the formation of caustics in Laue diffraction [17]. The studies above all involve the spatial characteristics, but also attempts to investigate the temporal parameter have been made earlier in special cases of X-ray [18,19] and neutron diffraction [20]. Some work has been carried out with modulated ultrasonic waves [21-24] impregnating an artificial time structure to the carrier wave.

In the case of neutron scattering the effect of energy exchange between a neutron and an acoustic phonon is observed, which stems from the fact that the neutron velocity is comparable with that of ultrasound wave. In such exchange the amount of the energy transmitted is rather small - for an ultrasound wave with a frequency of 100 MHz it is approximately 400 neV. Studying the efficiency of energy exchange at the diffraction of

thermal neutrons is therefore an involved task calling for special methods. The authors of work [25] observed very weak extra peaks (angular satellites) in the proximity of the main reflection peak, which were caused by the energy exchange at the grazing diffraction of neutrons in a quartz single crystal on the grating of the surface acoustical wave. Impressive experiments have been performed to elucidate the concept of particle-wave dualism [26]. The authors observed the energy exchange of ~ 10 neV and the transition from quantum-mechanical to classical behavior.

In the chapter the neutron interactions with acoustic waves in solids observed by diffraction modern methods is discussed. Fundamental questions such as the investigation of the diffraction process itself as a response to the ultrasonic field as well as its applications to beam optics or materials research are of interest.

2. Diffraction on a perfect crystals Laue geometry

2.1. Theoretical background

The theoretical problem of ultrasonic influence on neutron and X-ray diffraction was under intensive investigation [8,9,16, 27,28]. Depending on the ultrasound acoustic waves (AW) frequency, a distinction can be made between two different physical mechanisms. At AW frequency $\nu_s < \nu_{res}$, where ν_{res} is the AW frequency at neutron-acoustic resonance condition (see below) dispersion surface (DS) varies insignificantly and the problem is solved in terms of the usual perturbation theory. The correction to the eigen functions are of the order of Hw (H is the reciprocal lattice vector, w the AW amplitude), and additions to the scattering intensity are of the order of $(Hw)^2$. Hence at sound frequencies $\nu_s < \nu_{res}$ there takes place nearly complete “pumping” of the elastic component of scattering into inelastic one. The Mossbauer diffraction spectra obtained on single Si crystal confirm the theoretical results [29,30]. The more interesting phenomena arise when the magnitude of the ultrasound wave vector k_s is of order or greater of the gap ΔK_0 between the branches of the DS (in the two-beam approximation). Interaction between modified Bloch states by means of high-frequency ultrasonic perturbation leads to new physical effects, such as the resonant ultrasonic suppression of the Borrmann transmission [31], the ultrasound induced *Pendellosung* beatings in diffraction intensity [14,32] and some another features. The effect of US (ultrasound) on neutron and X-rays diffraction in a perfect crystal is schematically shown in Fig. 1. The new energy gaps k_s appear on DS which correspond to the additional regions of total reflection for the case of Bragg geometry. The US phonon’s absorption (emission) by neutron mixes Bloch states [33] and displaces the dispersion surface of the neutron by the value of quasi-momentum δq :

$$\delta q = \nu_s / (v_n \cos \theta_B) \pm k_s. \quad (1)$$

The neutron-acoustic resonance frequency ν_{res} is determined by expression (2)

$$\nu_{res} \approx (v_n \cos \theta_B) / \tau \quad (2)$$

where θ_B and v_n are the Bragg angle and the neutron velocity, and τ is the extinction length. Expression (1) is valid, if $H \perp k_s$ and this corresponds to the conditions of transversal AW. Taking into account the Debye–Waller factor, v_{res} does not depend on the observed reflection [16]. For the case $v_s > v_{res}$ a linear increase in the diffraction intensity should be observed depending on the US wave’s amplitude w [14].

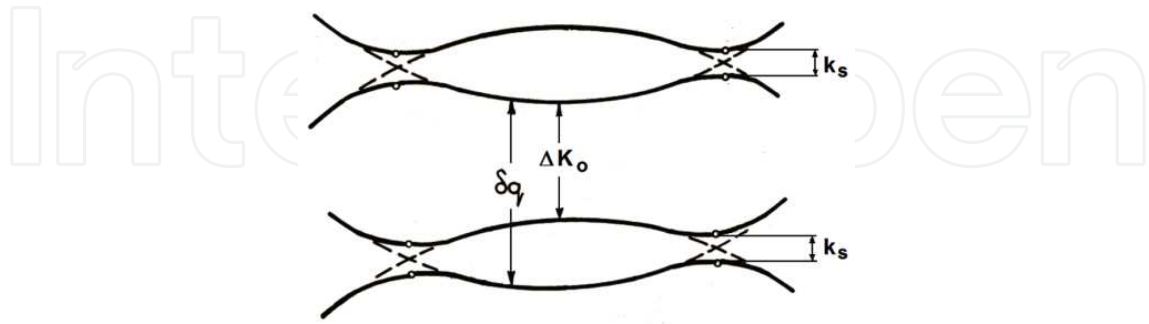


Figure 1. Schematic image of the dispersion surface modified by ultrasound in a perfect crystal (Laue geometry): ΔK_0 is the gap between the sheets of dispersion surface determining the resonance frequency ($\tau = 2\pi/\Delta K_0$); and k_s are the new US energy gaps determining the additional regions of Bragg reflection.

The change in the diffracted neutrons intensity distribution for the crystal by the AW can be interpreted quantitatively and qualitatively by the dynamical diffraction theory. Calculations taking into consideration the strains created by AW which affect the neutron wave field inside the crystal can be carried out using the Takagi–Taupin equations [34,35]:

$$i\beta \frac{\partial \Psi_0}{\partial t} = -i \frac{\partial \Psi_0}{\partial z} - i \tan \Theta_B \frac{\partial \Psi_0}{\partial x} + \frac{\Delta k_0}{2} \exp(iHu) \Psi_h \tag{3}$$

$$i\beta \frac{\partial \Psi_h}{\partial t} = - \frac{\partial \Psi_h}{\partial z} + i \tan \Theta_B \frac{\partial \Psi_h}{\partial x} + \frac{\Delta k_0}{2} \exp(-iHu) \Psi_0 \tag{4}$$

where

$$\beta = 1 / (v_n \cos \Theta_B)$$

and

$$u = w \cos(\omega t) \cos(k_s z) \tag{5}$$

is the displacement of the nucleus for standing transverse waves excited between the two parallel surfaces of the sample with waves amplitude w , wave-length λ_s , wave vector $k_s = 2\pi / \lambda_s$. Ψ_0, Ψ_h are the amplitudes of the incident and diffracted beams, respectively, v_n is the velocity of the neutron wave and $\Delta K_0 = 2\pi / \tau$ where τ is the extinction length. The full solution of the Takagi–Taupin equations isn’t possible now but some approximations can be done and this allows calculating diffraction intensities at the center of the Bormann fan in the quasi-classical approximation depending on w, k_s, λ_n and τ .

2.2. Experimental

The experimental layout for Laue geometry is shown in Fig. 2. As the sample, a Ge ((111) reflection single crystal ($V= 52 \times 22 \times 20 \text{ mm}^3 = Y \times L \times T \text{ mm}^3$) was taken. A monochromatic and well-collimated neutron beam with a cross section of $1 \times 10 \text{ mm}^2$ was directed to the sample. The sample quality was checked preliminarily and the FWHM of the rocking curve was $3.1''$, close to the theoretical expectation. For the observation of the diffracted neutrons distribution two techniques were used. One of them using analyzing slit similar to the classic experiments [36-38] but with width 0.5 mm in difference of 0.1 mm slits in [36] to avoid “non-sound” intensities oscillations (Shull’s fringes). At other method an analyzing slit was not used in general. Instead, the spatial distribution of the reflected neutron beam was measured with a position sensitive detector (PSD) After finding the optimal relation $\Theta - 2\Theta$ (adjustment) the sample and PSD were kept motionless and the reflected intensity distribution was directly measured in 2Θ – coordinates then recalculated for current x -coordinates . This procedure is similar to the scanning with slit method, however, if PSD has good resolution enough, allows a much faster data acquisition.

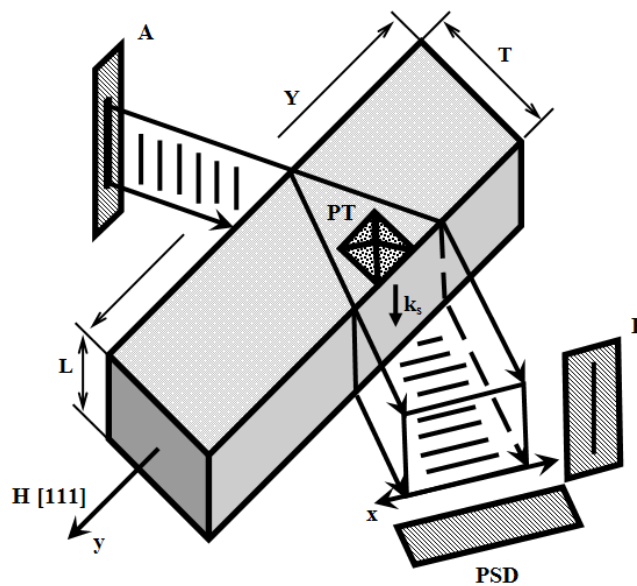


Figure 2. The layout of the experiment: A and B are forming and analyzing slits, respectively; PSD is position sensitive detector; PT is a piezo transducer; H is the vector of the reciprocal lattice; k_s is AW wave number; y is direction of samples movements (slit B is not moving), x is a current coordinate in the base of Borrmann’s fan and a direction of slit B movement. In this case, the sample is not moving.

2.3. Acoustic field in the sample

The transverse AW propagated perpendicular to the scattering vector ($k_s \perp H$, $u \parallel H$). Polarized AW with amplitude w was parallel to the vector H. Piezotransducer was glued to the sample by salol. As shown below, the diffraction intensity is proportional to $|Hw|$, where w is the AW amplitude, therefore its values could be used for estimation of the acoustic field inside the crystal. Owing to the diffractive divergence of acoustic waves this

field is concentrated not only in the region around the piezotransducer but is distributed uniformly enough through the whole sample, especially at the levels of the weak and moderate excitation.

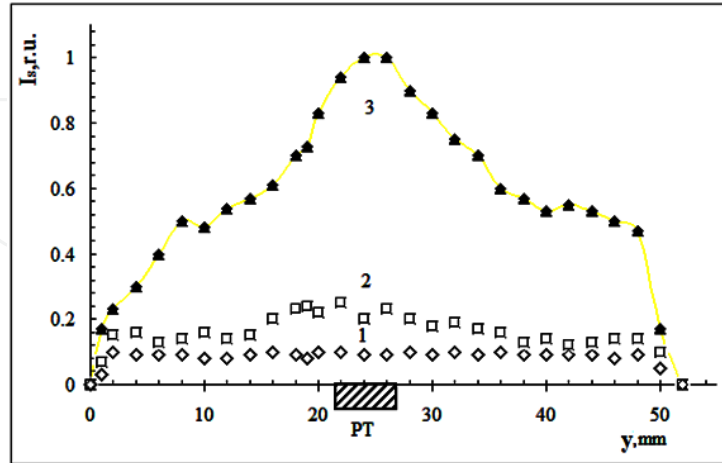


Figure 3. Diffraction intensity distribution in relative units at sample displacement along y-axis: 1 - in the absence of ultrasonic excitation; 2 - $V_G=0.1V$; 3- $V_G=0.8V$. The I_s value is proportional to the AW amplitude.

The uniformity of acoustic field distribution in the region of Borrmann's fan is an important prerequisite to a sure observation of spatial oscillations of the diffraction intensity (see below). Assume that in the diffraction process a finite volume of the sample participates, in which the amplitude w of AW oscillations is distributed in the interval $w \pm \Delta w$. This leads to a smearing of the pulse ($k_s \pm \Delta k_s$), therefore the phase difference on the crystal surface will be $\Delta\varphi = \Delta k_s T = \Delta k_0 H T (w \pm \Delta w)$. Since the intensity oscillations are approximately described by the function $I \sim \cos^2(\Delta k_s T)$, the n -th intensity maximum corresponds to the condition $\Delta\varphi = \Delta k_0 H w T$. At a phase shift of $\Delta\varphi_1 = \pi/2$ the maximum of I_s becomes its minimum. Therefore, to observe oscillations it is necessary that the phase shift $\Delta\varphi_1$ be less than $\pi/2$. From this follows the estimation $\Delta w/w < 1/2n$. At reasonable w values and $\Delta w/w \approx 10\%$ this leads to the situation when in the experiment only few first oscillations could be observed (see below). From the data shown in Fig. 3 it is seen that these conditions are fulfilled well at low amplitudes of AW (curve 2, Fig. 3).

2.4. Acoustic waves velocities

The evidence of the standing AW existence in the single crystals is shown on the Figs. 4 and 5 (a-c). As a rule, theoretical estimations of the AW effect on the diffraction intensity were made for the case of coherent sound. As follows from Fig. 4a, in our experiment a wide enough frequency spectrum of excitations and AW cannot be considered as single mode. However, as was previously shown [28], the assumption of sound coherence is not always necessary for the correct interpretation of experimental results. When the diffraction intensity depends on frequency under scanning with a smaller step (Fig. 4b), a fine structure appears which is the evidence of the presence of an AW standing wave in a crystal. When

the diffraction intensity depends on frequency under scanning with a smaller step (Fig. 4b), a fine structure appears which is the evidence of the presence of an AW standing wave in a crystal. For AW standing waves the relation

$$L=i\lambda_s/2 \quad (6)$$

should be fulfilled, where i is an integer of AW half-waves, λ_s is the AW wavelength, and L is the distance of wave propagation (Fig.2). Knowing L and the distance between the maxima (minima) of the fine structure of the frequency dependence $\Delta v_s = [v_{si} - v_{s(i\pm 1)}]$ (Fig. 4b), it is possible to determine the velocity of sound propagation in the [100] direction. Determining $\Delta v_s = (0.08 \pm 0.01)$ MHz from Fig. 4b data we obtain $i = 517-524$, which is testimony to a very high quality of the sample, and $v_{s[100]} = (3.52 \pm 0.03) 10^5$ cm/s. This value is in very good agreement with the reference data $3.55 \cdot 10^5$ cm/s [36] for the velocity of a shear AW for Ge in the indicated direction.

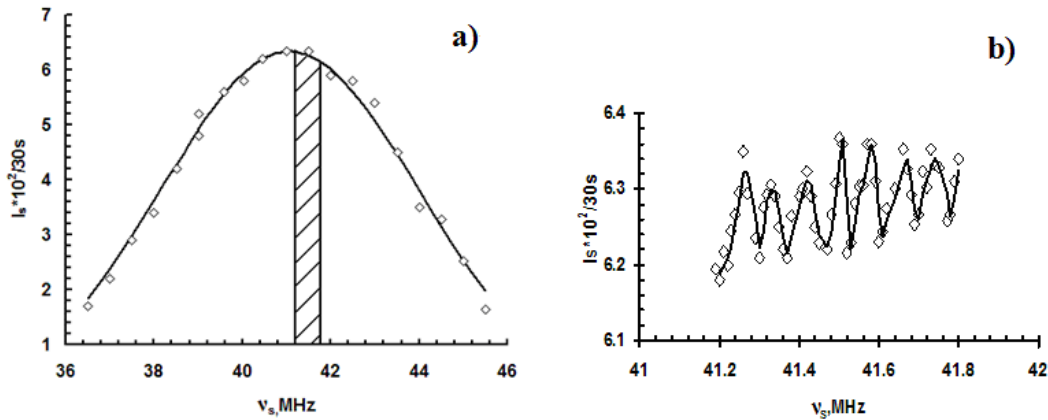


Figure 4. Dependence of the Laue diffraction's intensity I_s at the Bormann's fan center on the ultrasound frequency ($\lambda_n = 0.410$ nm, $S = 1$ mm, $L = 22$ mm): a) the frequency scanning step is 0.5 MHz; the solid curve is a result of data fitting by Gaussian with FWHM = 6.34 MHz; the region in which the detailed frequency scanning was carried out is shaded (41.2-41.8 MHz); b) the same as in (4a) only for the narrow frequency range, shown in the Fig. 4a as a shaded. The frequency scanning step is ~ 0.01 MHz; the solid curve was obtained using the averaging on three points data (spline approximation).

The presence of frequency satellites shown in Fig. 5(a-c), which exist at equal distance from the main peak independently of the chosen frequency interval, is the one more evidence for excitation of standing waves in the crystal. And the sound velocity v_s in the [111] direction parallel to the scattering plane can be determined. Defining Δv_s from the dependences shown in Fig. 5a-c, where $\Delta v_s = (1.475 \pm 0.046)$ MHz one can see that the number of transverse half-waves $i = 10-12$ for $v_s = 14.84$ MHz and $v_{s[111]} = 5.13 \cdot 10^5$ cm/s. This value is very close to the reference data of $5.09 \cdot 10^5$ cm/s [39]. This means that the values of US wave velocities in crystals can be determined with neutron and X-ray diffraction technique, and that this method is applicable for, e.g., determination of the sound velocity at phase transitions.

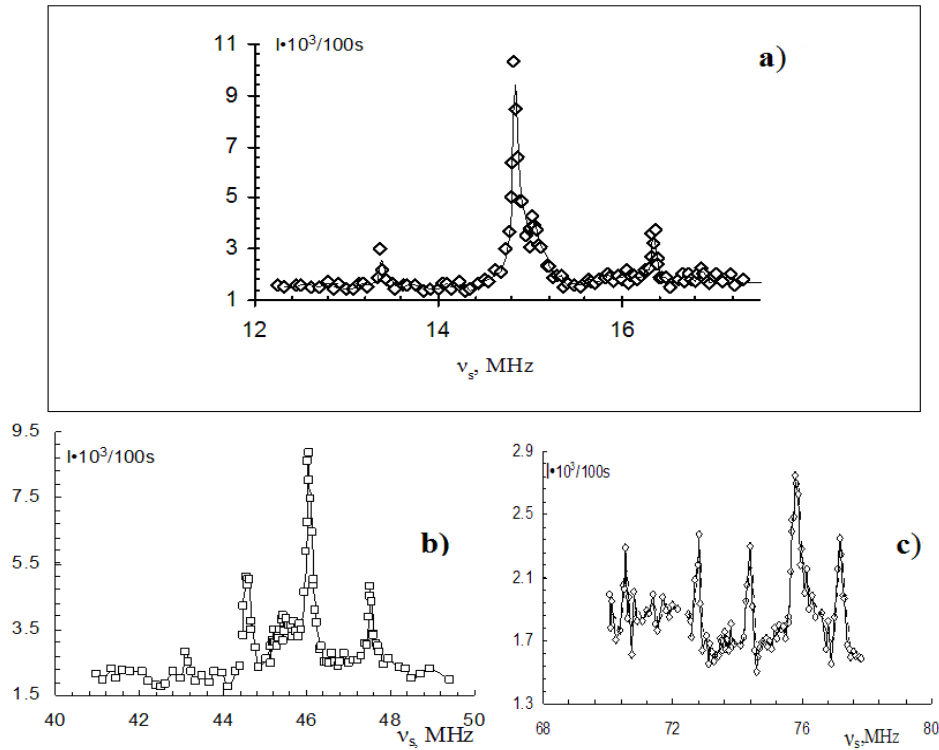


Figure 5. Standing AW observation in the single thin Si crystal ($T=1.73$ mm):a) for main transducer harmonic (15 MHz); b) the same for third harmonic; c) the same for fifth harmonic. Solid curves were obtained using the averaging on three points data (spline approximation).

3. Spatial intensity distribution of diffracted neutron beam

Owing to the interference of Bloch's waves the distribution of diffracted neutron beam intensity in a crystal arising on its outside surface has characteristic beats at the center and intensity is increasing toward the edges of the Bormann fan. These effects are described by the expression (7) [40]:

$$I_0(\Gamma) = c(1 - \Gamma^2)^{-1/2} \cos^2(A(1 - \Gamma^2)^{-1/2}) \quad (7)$$

where $\Gamma = x/(2T \operatorname{tg} \Theta_B)$ is the deviation of a neutron wave from the atomic plane trace; $A = \pi T/\tau$; c is a normalized constant, and x is a current coordinate in the base of Bormann's fan. Expression (7) is valid for the diffraction of a plane monochromatic wave in the symmetrical Laue case. A more rigorous expression for the shape of the reflected beam distribution can be obtained with the help of spherical neutron waves [40,41]:

$$I_0(\Gamma) = \frac{A}{2} J_0^2(A\sqrt{1 - \Gamma^2}) \quad (8)$$

where J_0 is Bessel function of the zeroth order. According to Exprs. (7,8) the intensity of a diffracted beam oscillates on the exit surface of a crystal, with the oscillation period depending on parameter $\pi T/\tau$ and fast decreases outward from the center of profile ($\Gamma=0$).

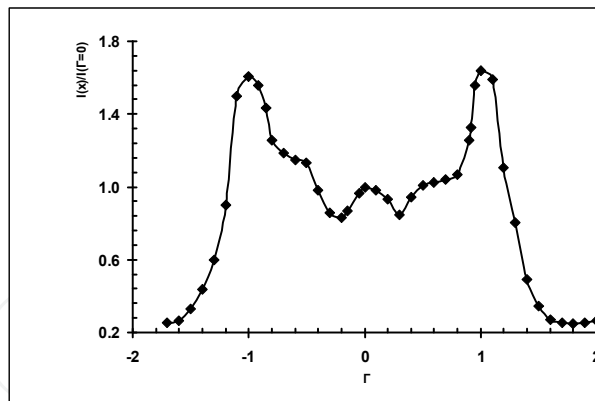


Figure 6. Normalized intensity distribution for Si single crystal (reflection reflex (111)), slit B width $S \leq 0.2$ mm. $T=11$ mm. Neutron wavelength λ_n is equal 0.1 nm. The Shull's fringe is clearly seen at the center of profile [42].

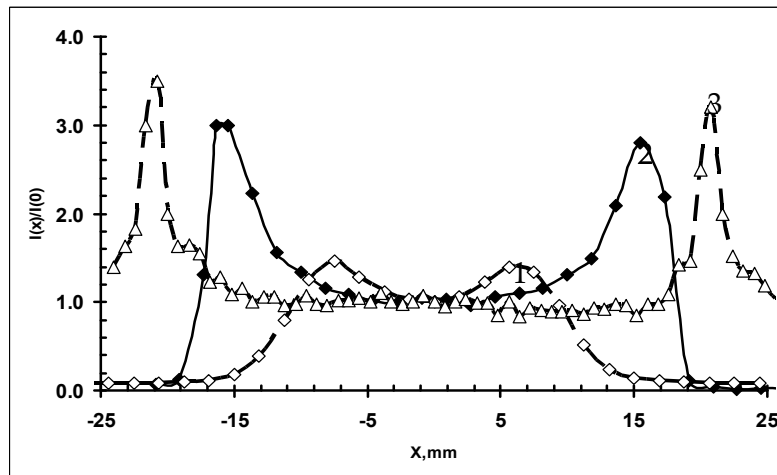


Figure 7. Normalized intensity distribution for reflection (111) Ge ($T=20$ mm) (Bormann fan) for different neutron wavelengths without sound: 1- $\lambda_n=0.471$ nm; 2- $\lambda_n=0.410$ nm; 3- $\lambda_n=0.243$ nm. Curve 2 was obtained using a slit with $S=1$ mm. Curves 1 and 3 were obtained without analyzing slit (PSD only).

3.1. High-frequency sound effect on the spatial distribution of diffracted neutron intensity

The presence of new energy gaps k_s (Fig. 1) on the dispersion surface under ultrasound should lead to the appearance of an additional structure in the intensity distribution of diffracted neutrons at the exit of a crystal. The new distribution, as is shown below, depends on the AW amplitude, w , while "sound" oscillations are superimposing on the initial ones. The size of the first soundless oscillation for the Ge (111) reflex according to formula (7) is $\Delta x_1 = (T \tau)^{0.5} t g \Theta_B \approx 1.5$ mm (in the vicinity of $\Gamma=0$). The numerical analysis of experimental data based on the known theoretical expressions involves difficulties, since they have been obtained in the plane neutron wave approximation. Such approximation cannot be applied to description of the intensity distribution of diffracted neutrons on the Bormann fan's base when the whole dispersion surface is excited.

We have derived expressions for the diffraction intensity of a spherical neutron wave in an ideal crystal under ultrasound excitation. In this case the total diffraction intensity I_t is composed of the elastic and inelastic components:

$$\begin{aligned} I_t &= I_{el} + I_{in} \\ I_{el} &= I_0 + \Delta I_{el} \end{aligned} \quad (9)$$

where ΔI_{el} and I_{in} are the elastic and inelastic addends, respectively; I_0 is determined from expression (8), while the elastic addend to the diffraction intensity is given by the expression (10):

$$\Delta I_{el} = \frac{2\Delta K_0^2 (Hw)^2 \sin^2(\delta q T/2) J_1^2 \left(AHw(1-\Omega)^{0.5} \right)}{\left(\delta q^2 - \Delta K_0^2 \right) (1-\Omega)} \quad (10)$$

where J_1 is Bessel function of the first order, δq is the shift of the DS at absorption or emission of an ultrasound phonon. The main contribution to the intensity of inelastic (one-phonon) scattering is made by the term:

$$I_{in} = (Hw)^2 \left(1 + \frac{\delta q^2}{\left(\delta q^2 - \Delta K_0^2 \right)} \right) J_0^2 \left[AHw(1-\Omega)^{0.5} \right] \quad (11)$$

where

$$\Omega = \frac{\Gamma^2 \delta q^2}{\left(\delta q^2 - \Delta K_0^2 \right)}, \quad A = \pi T / \tau \quad (12)$$

Formulas (10-12) describe the central part of a Bormann fan:

$$-\left(1 - \Delta K_0^2 / \delta q^2 \right)^{0.5} \leq \Gamma \leq \left(1 - \Delta K_0^2 / \delta q^2 \right)^{0.5} \quad (13)$$

besides, these are valid at $\Delta K_0 Hw \ll (\delta q - \Delta K_0)$, which corresponds to the weak interaction of satellites with the main Bragg maximum. At $v_s \gg v_{res}$, ($\delta q \gg \Delta K_0$), i.e. under the conditions of our experiment, I_{in} far exceeds ΔI_{el} , which was previously confirmed by our experiments with measuring the spin-echo in a silicon single crystal under ultrasound pumping [43]. The spatial distribution of diffraction intensity is described by the expression:

$$I_s(\Gamma, Hw) = I_0 + I_{in} \quad (14)$$

where I_{in} is taken in the form of equation (11), and I_0 – of equation (8). The general character of the spatial distribution of diffraction intensity is dictated by three parameters: A , Hw , and the $\delta q / \Delta K_0$ ratio. The choice of a thick ($T \approx 70 \tau$) Ge crystal is not quite optimal, since the first AW

oscillations will appear when the “acoustic” extinction length becomes equal $\tau_s = \tau |Hw|^{-1}$. On the other hand, a thick crystal provides long enough Bormann fan, which allows for easy and detailed measurements of the spatial distribution of diffracted beam intensity (see Fig. 8)

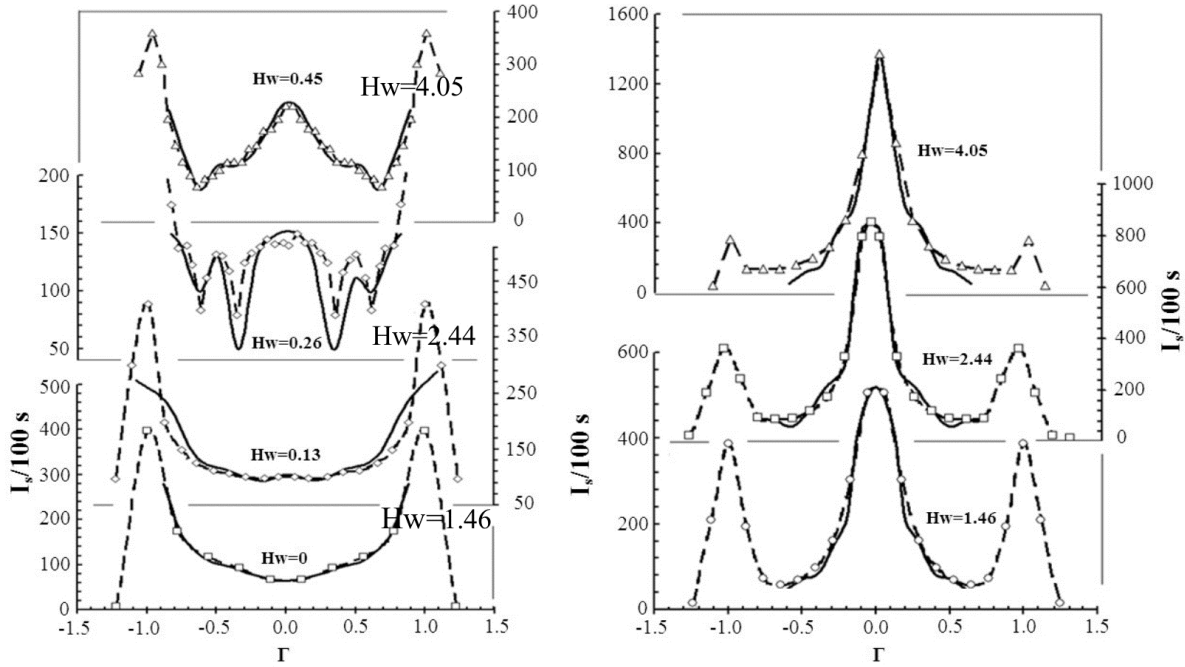


Figure 8. Spatial distribution of a diffracted beam intensity vs AW amplitude w and Γ value. Dashed curves and points – averaged experimental data, solid curves is a result of data fitting by Exprs. (11 and 8)

Already at a small amplitude of the acoustic wave $Hw=0.26$ ($w=0.013$ nm) the diffraction intensity in the center starts rising noticeably. The width of the first oscillation (Fig. 8) on the x -axis (close to $\Gamma=0$) at $Hw=0$ could be estimated from expression (8): $\Delta x_1 = (2T\tau)^{1/2}tg\Theta_B$ and $\Delta x_1 \approx 6$ mm for the Ge (111) reflex. Since at the appearance of sound a new extinction length is $\tau_s = \tau |Hw|^{-1}$, at $Hw \ll 1$ the linear size of the first “sound” fringe will be increasing as $\Delta x_s = \Delta x_1 |Hw|^{-0.5}$. As follows from Fig. 8, at $Hw=0.26$ the length of the first acoustic fringe is 11.4 mm, which coincides well with the calculated value of 12 mm. Besides, at least two next oscillations could be clearly discerned. As Hw is further increasing, at the profile center a linear intensity rise is observed, while the diffraction intensity on the Bormann fan edges ($\Gamma = \pm 1$) remains practically unchanged. To compare the theoretical and experimental data a high-precision determination of the A and Hw parameters is needed, since the Bessel function is fast oscillating at large values of the argument. The calculated A value is 2071, i.e. close to $A=2060$, at which “soundless” distribution of the diffraction intensity ($Hw=0$) is described most satisfactorily by expression (8), taking into account integration over the width of analyzing slits and correct averaging. The AW amplitude can be determined by changes in relative intensity variations at the center of the spatial profile ($\Gamma=0$):

$$\eta = \frac{I_s - I_0}{I_0} = \frac{I_{in}}{I_0} = \frac{(Hw)^2 \left[1 + \delta q^2 / (\delta q^2 - \Delta K_0^2) \right] J_0^2(HwA)}{J_0^2(A)} \quad (15)$$

At large values of argument

$$J_0(z) \rightarrow \sqrt{2/\pi z} \cos(z - \pi/4), \tag{16}$$

and the relative contribution of the neutron inelastic scattering by AW of the lattice with a frequency above resonant is:

$$\eta(Hw) = 4Hw \frac{\cos^2(HwA)}{\cos^2(A)} \approx 4Hw \tag{17}$$

The experimental data shown in Fig. 9 were obtained for one and the same sample but on different neutron diffractometers using different RF-generators and wide-band amplifiers. Besides, every time the piezotransducer was glued again; however, in all cases a linear dependence of η on the generator voltage V_G was observed, which makes it possible to find a calibration constant C and to determine the AW amplitude w from the relationship: $\eta = C |Hw|$.

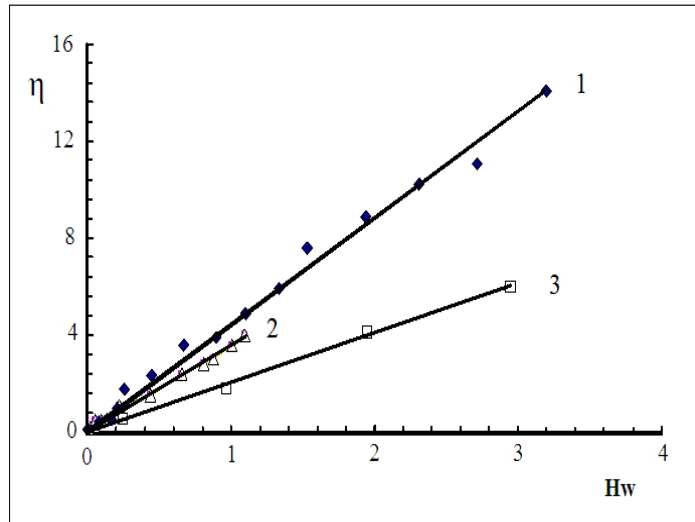


Figure 9. Diffraction intensity at the center of a Bormann fan ($\Gamma=0$) vs. acoustic wave amplitude for neutrons of different wavelength: 1) $\lambda_n=0.41$ nm; 2) $\lambda_n=0.471$ nm; 3) $\lambda_n=0.243$ nm. Solid curves: fitting with eq.(18) taking into account $\nu_s \gg \nu_{res}$ ($\Delta K_0 \ll \delta q$)

The effect of saturation was observed in the η dependence versus V_G for large Hw . The heating of the organic salol gluing leads to the decrease of its viscosity and brings about violation of the proportionality between V_G and w . This fact was taken into account, and the measurements were considered reliable up to $Hw \leq 5$

Fig. 10 shows the spatial distribution of diffraction intensity I_t depending on the acoustic wave amplitude for the neutrons of different wavelength. Independently on the neutron waves length, I_t at the Bormann fan centers increases with Hw growth.

Figure 11 demonstrates a sharp decrease in the spatial half-width of the central peaks in dependence on the AW amplitude. This result seems to be unexpected, since in some earlier works where the possibility to create the ultrasound-driven/controlled monochromators was discussed [12,27,44] the gain in intensity with rising AW amplitude is always compensated by a loss in resolution (due to FWHM rise). In contrast, in our experiments the FWHM *decreases* 3-4 times at the *Hw* increased twice. To study this effect in more detail, additional investigations are needed – for example, measuring the FWHM of double-crystal rocking curves in dependence on the *Hw* at the center of Bormann's fan.

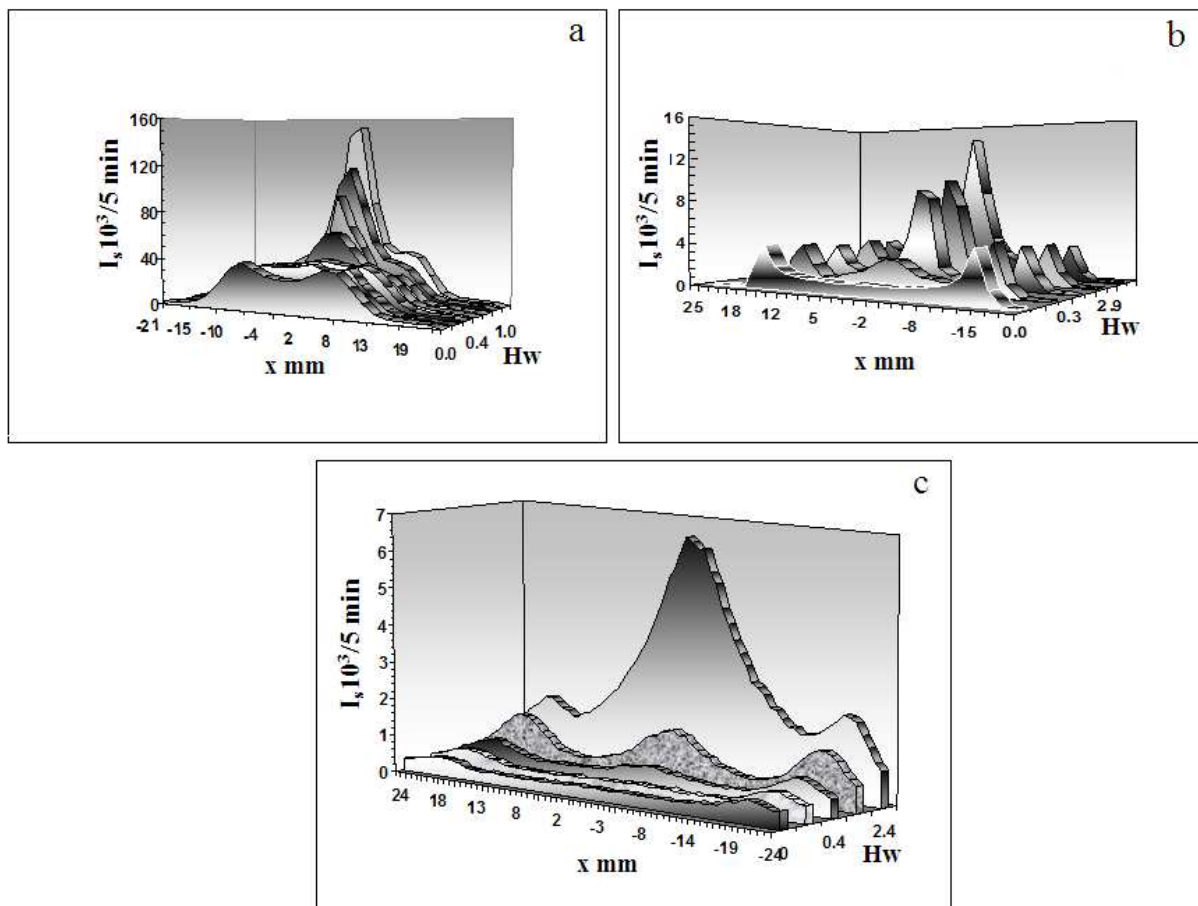


Figure 10. The neutron diffraction intensity as a function of acoustic wave amplitudes Hw and running coordinate x in the base of a Bormann fan for neutrons of different wavelength: a) $\lambda_n = 0.410 \text{ nm}$; b) $\lambda_n = 0.243 \text{ nm}$; c) $\lambda_n = 0.471 \text{ nm}$.

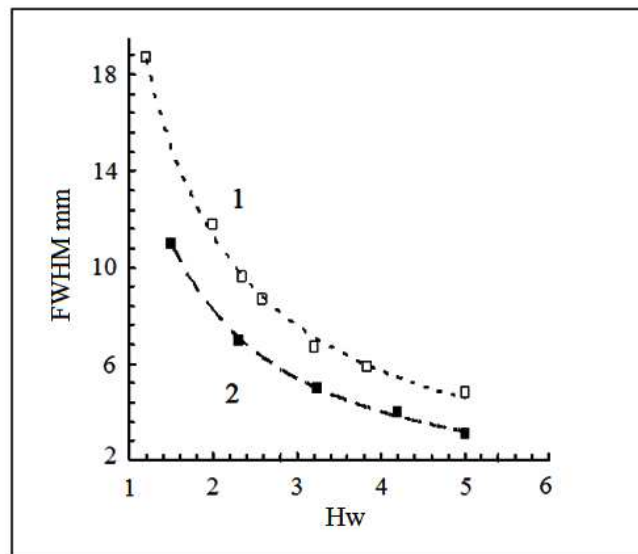


Figure 11. Full width at half maximum of the central peaks vs AW amplitude for neutron with different waves length: 1) $\lambda_n=0.410$ nm, 2) $\lambda_n=0.243$ nm

4. Diffraction - Deformed crystal

4.1. Theoretical background

In contrast to a perfect crystal where the US effect leads, as a rule, to an increase in the diffraction intensity, in a bent smoothly deformed sample a drastic decrease in the intensity I_{ds} is observed already for very small AW amplitudes. In deformed crystals, which are of great practical interest, the effect of US on diffraction has been investigated much less. In [14, 45, 46] the results of theoretical and experimental investigations of neutrons and X-rays for the case of Laue diffraction in deformed silicon single crystals under high-frequency ($v_s \gg v_{res}$) and in conditions of the neutron (X-ray) - acoustic resonance ($v_s \approx v_{res}$) are reported. The analysis has shown that in a deformed Si crystal ultrasound results in violation of the adiabatic conditions for the movement of tie points on the dispersion surfaces. Owing to this, a drastic decrease in the diffraction intensities was observed for low acoustic wave amplitudes. With the AW amplitudes increasing the diffraction intensity also increases, reaching the kinematical limit. In absolute values, the influence of the US is much stronger manifested in the diffraction on a deformed crystal than on a perfect one. A substantial role is played by multiphonon processes. The presence of static strains leads to the appearance of a new type of oscillations, which depend on the deformation gradient.

As distinguished from the perfect crystal case where for the whole crystal a unitary DS exists, in the Penning–Polder–Kato model [47,48] to each point of a bent crystal an own two-sheet dispersion surface corresponds, and the neutron is travelling adiabatically inside the crystal without transitions of the excited tie point between the effective DS sheets (Fig. 12)

The role of ultrasound in this model consists in the resonant suppression of adiabatic movement of the tie points. The one-phonon absorption corresponds to path 1–2–6–7–8 of the tie point along the dispersion surface. The neutron incident on the crystal excites points 1

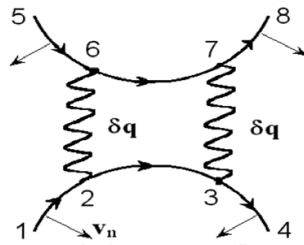


Figure 12. Dispersion surfaces of a crystal modified by ultrasound. Dynamics of travelling of tie points in a deformed crystal. Laue geometry. Directions of tie points and neutron group velocities are shown by arrows.

and 8 on the DS. In the absence of ultrasound, point 1 travels along path 1–2–3–4 and passes into the state corresponding to a diffracted wave. Point 8 makes no contribution to the diffraction. When US is switched on, the movement of point 8 is not disturbed. As concerns point 1, it can reach state 4 by two ways: a) 1–2–6–7–3–4 or b) 1–2–3–4. If the probability for the excitation point to remain on DS sheets at points 2, 3, 6, and 7 is P , and the probability to pass onto another DS sheet owing to the US disturbance is M ($P+M = 1$), then the probability of the former process is equal to M^2 , the probability of the latter process is equal to P^2 . The change in the relative diffraction intensity will be

$$\eta = (I_{ds} - I_{d0}) / I_{d0} = P^2 + M^2 - 1 = -2MP < 0. \quad (18)$$

The probability of transition for the excitation point 1 in the case of Laue's diffraction is approximately described as

$$M = 1 - \exp[-\pi(Hw)^2 / 2B] \quad (19)$$

where B is the deformation gradient .

The maximum transition probability is 0.5, (for $v_s > v_{res}$) and, correspondingly, $\eta_{max} = 0.5$ according to expression (19). Interference between the trajectories of the two scattering process leads to the oscillating dependence on B^{-1} of the maximum "dip" of the diffraction intensity. These oscillations modify the expression (19) as follows:

$$\eta = -2MP(1 - \cos 2\varphi) \quad (20)$$

with phase factor φ [14]:

$$\varphi = (a/B)(a^2 - 1)^{0.5}; a = k_s / \Delta K_0 \quad (21)$$

For the Laue-symmetrical diffraction of neutrons and X-rays in a two-wave approximation when the propagation of neutron waves in a crystal with static and/or dynamic (US) deformations is described by the Takagi-Taupin equations (Expr. 3-5), where the displacement of nuclei, u , is introduced in forms [46]

$$\begin{aligned} Hu &= Hu_s + Hu_d \\ Hu_s &= 4Hw \cos[k_s(s_0 + s_h) \cos \Theta_B] \cos(\omega_s t) \end{aligned} \quad (22)$$

$$Hu_d = 2as_0^2 + 4bs_0s_h + 2cs_h^2 \quad (23)$$

$$B = b[2/(\Delta k_0 \cos \Theta_B)]^2 \quad C = c[2/(\Delta k_0 \cos \Theta_B)]^2$$

where a , b , and c are numerical constants describing inhomogeneous deformation; u_s is the nuclear displacement in the acoustic field, and u_d is the nuclei static displacement associated with the lattice deformation.

In the quasi-classical approximation ($B \ll 1$ but $BT \gg 1$), for $Hw < 1$ we will have analytical expressions (24-26) obtained by method of successive approximations for relative intensity variations depending on the relationship between k_s and k_0 . If the frequency of acoustic waves ν_s is higher than the resonance frequency ν_{res} , ($\alpha > 1$) the second term in (26) describes the so-called "deformations oscillations" whose period depends on B and α .

$$\eta = 1 - \frac{I_h(Hw, B)}{I(0,0)} = \frac{\pi[Hw \cos(\omega t)]^2}{B[8(1-\alpha)]^{1/2}} \times \exp\left(-\frac{2^{5/2}(1-\alpha)^{3/2}}{3B}\right) \quad \alpha < 1 \quad (24)$$

$$\eta = \frac{(Hw \cos(\omega t) \Gamma(1/3))^2}{\pi B^{4/3}} \quad \alpha \gg 1 \quad (25)$$

$$\eta = \frac{\pi[Hw \cos(\omega t)]^2 \alpha}{B(\alpha^2 - 1)^{1/2}} \times \left[1 + \sin\left(\frac{(\alpha^2 - 1)\alpha}{2B} + \operatorname{arcsinh}(\alpha^2 - 1)^{1/2}\right) \right] \quad \alpha > 1 \quad (26)$$

where $\alpha = k_s / \Delta k_0$.

The experimental verification of the qualitative validity of expressions (23-26) is presented on the Figs. 13-15

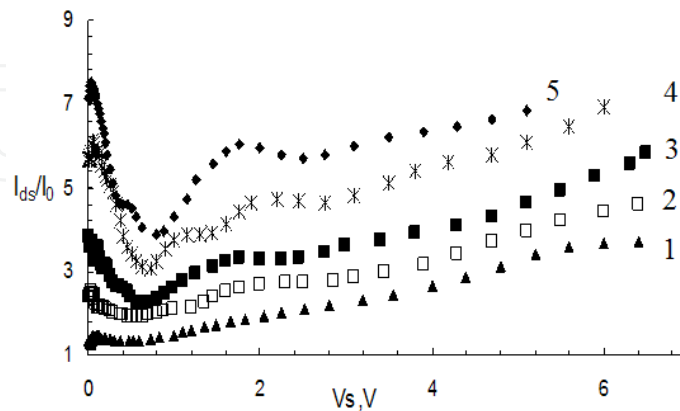


Figure 13. Variations in the relative intensity of diffraction in a deformed crystal *vs.* voltage on piezotransducer for $\alpha = 3.13$ ($\nu_s = 46.04$ MHz) and different B : 1 – 0.023 (\blacktriangle); 2 – 0.052 (\square); 3 – 0.083 (\blacksquare); 4 – 0.124 ($*$); 5 – 0.166 (\blacklozenge); I_0 is the diffraction intensity in a perfect crystal without sound; I_{ds} the same for a deformed one.

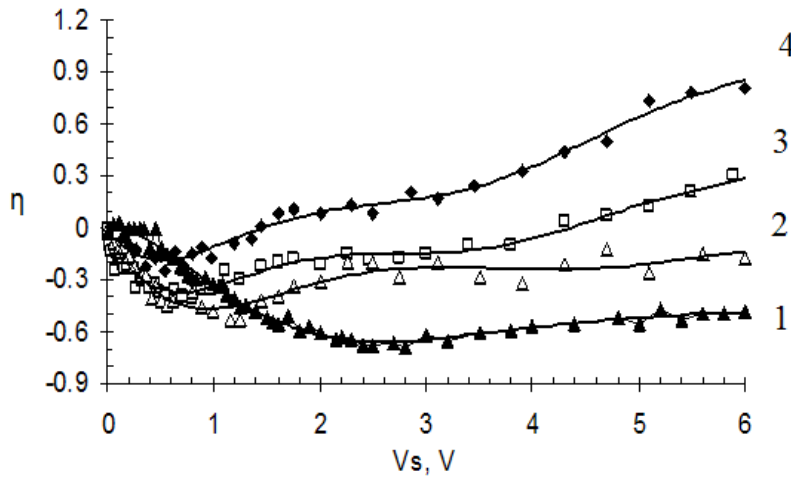


Figure 14. Relative diffraction intensity vs. piezo transducer voltage for different values of parameter B : 1) -0.06 , 2) -0.11 , 3) -0.23 , 4) -0.89 ; $\nu_s=14.84$ MHz ($\alpha \approx 1$). The best fitting is obtained using series expansion of the Bessel functions $J_0 \left[\frac{(HW)^2}{B^{4/3}} \right]$ (solid curves).

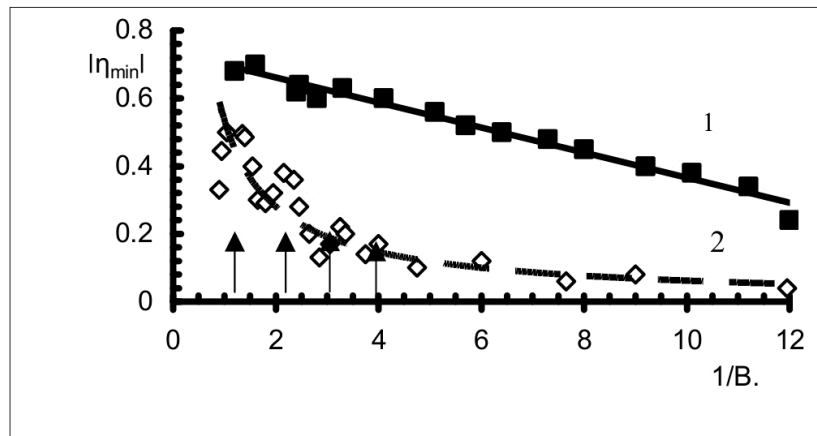


Figure 15. The module of “dip” maximum depth $\eta = |I_{ds} - I_{d0}| / I_{d0}$ vs. the inverse value of the deformation gradient B : 1(■) – for $\nu_s = 14.84$ MHz (near to neutron acoustic resonance, $\nu_{res} = 14.71$ MHz; $\alpha \approx 1$); 2(◆) – for $\nu_s = 46.04$ MHz; $\alpha \approx 3$. Arrows show the maxima positions calculated by Eqs. 20 and 21

The solid (1) and dashed (2) curves in Fig. 15 were obtained from experimental data by the least squares method. The best fitting is at $|\eta_{min}| = 0.53 \cdot (1/B)$ for curve (2) and $|\eta_{min}| = -0.04B^{-1} + 0.74$ for curve (1). From these it follows that at $B \sim 1$ the “dip” of the relative diffraction intensity η reaches the maximum of ~ 0.5 for $\nu_s \gg \nu_{res}$ and of 0.7 for $\nu_s \approx \nu_{res}$. The strong effect near the neutron-acoustic resonance ($\alpha \approx 1$) follows from Eq. 25 and by analogy with the resonance destruction of Bormann’s effect [31] at the X-ray – acoustic resonance can be qualitatively explained by the fact that the transitions between DS branches in the case of their contact occur in a much greater volume of the pulse space.

4.2. Ultrasound effect on neutron bragg diffraction in a deformed silicon single crystal [23]

The scheme of the bending device, the neutron scattering geometry, and the US wave's propagation direction are shown in Fig. 16. The (220) and (440) reflections intensities were simultaneously measured at a standard single-crystal spectrometer by the time-of-flight technique [15]. The neutron wave lengths were 0.96 and 1.92 Å. The radius of curvature R of the reflecting surface was determined by sag h measured by a micrometer ($R=L^2/8h$), where L is the sample length equal to 12 cm. A sag was measured from 0 to 40 μm and R from 6 km to 51 m.

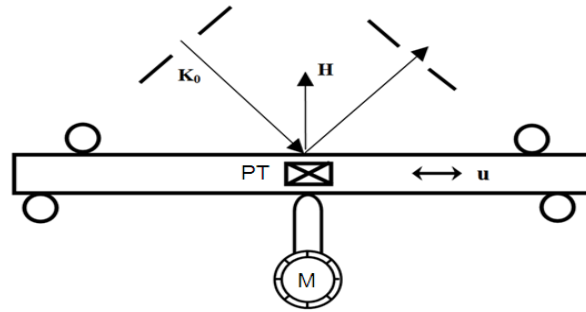


Figure 16. Scheme of experiment: H is the reciprocal lattice vector; K_0 is the wave vectors of neutron and ultrasound wave. $u=w \cos(\omega st) \cos(k_s x)$ is nuclei displacement in a US wave with amplitude w . PT is piezotransducer. M is micrometer. $R=L^2/8h$, where $L=12$ cm is a samples length, h is the sag.

The transversal US wave ($k_s \perp K_0, H \parallel w; w \parallel H$), where H is the reciprocal lattice vector, k_s and w are the US wave vector and amplitude, was excited in the [111] direction by a LiNbO_3 piezo transducer glued to the sample by salol. The fundamental piezoelectric transducer harmonic ($\nu_s= 26.5$ MHz) was used. Fig. 17 shows typical plots of the relative diffraction intensities $\eta=(I_s-I_0)/I_0$ vs the piezo transducer voltage for the two reflections (220) and (440) in the “perfect” crystal (without bending). It is seen that linear dependence is a good approximation.

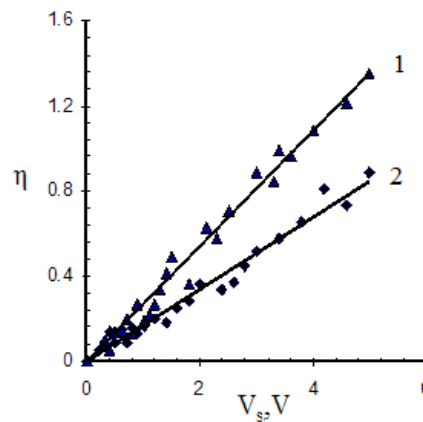


Figure 17. Relative changes of the diffraction intensities $\eta = (I_s - I_0)/I_0$ for perfect crystal for two reflections: 1-(▲) for (440), 2-(◆) for (220)

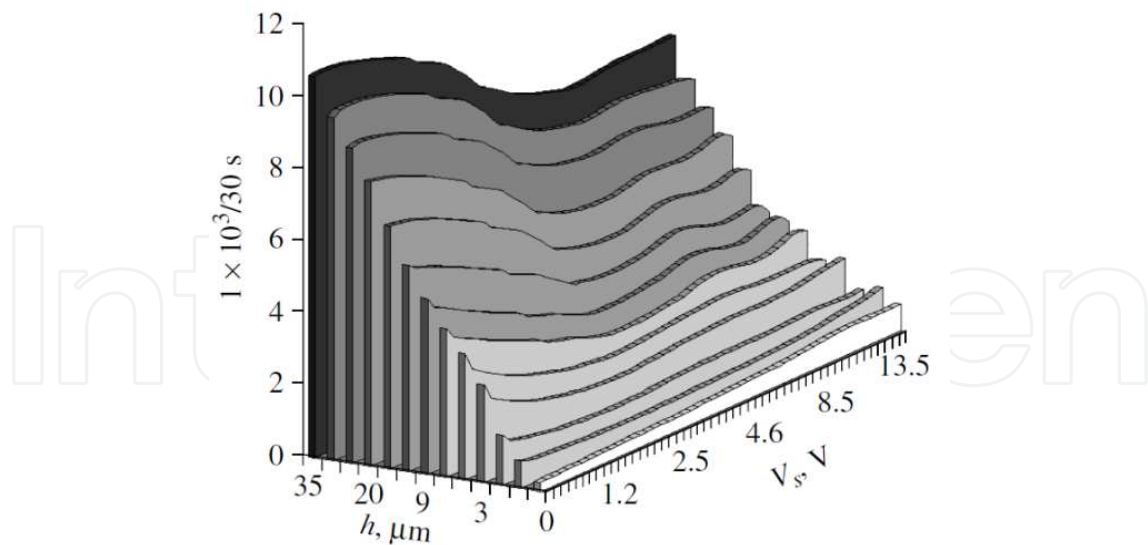


Figure 18. Common result of the simultaneous effect of ultrasound wave and bending of a crystal on the diffraction intensity of neutrons.

The total change in the intensity I_{ds} with a simultaneous increase in V_s and h is shown in Fig. 18. The appearance of dips (minima) in these dependences is a characteristic phenomenon similar same as for Laue case. The changes in I_{ds} (440 reflection) as a function of V_s are shown in details in Figs. 19a and b for a bent crystal for different values of the sag h . Instead of the linear increase in I_{ds} for $h = 0$ (line 1), a dip in I_{ds} reaches 30% for $h = 0.3 \mu\text{m}$ ($R \approx 51 \text{ m}$) at $V_s = 1.1 \text{ V}$ ($w \approx 0.05 \text{ \AA}$) (curve 2). With a further decrease in the bending radius the dip depth reaches the maximal value of 52% (Fig. 19a, curve 3), flattening out (Fig. 19b, curves 3–10). Curve 11 demonstrates the shift of the I_{ds} minimum over V_s with an increase in h .

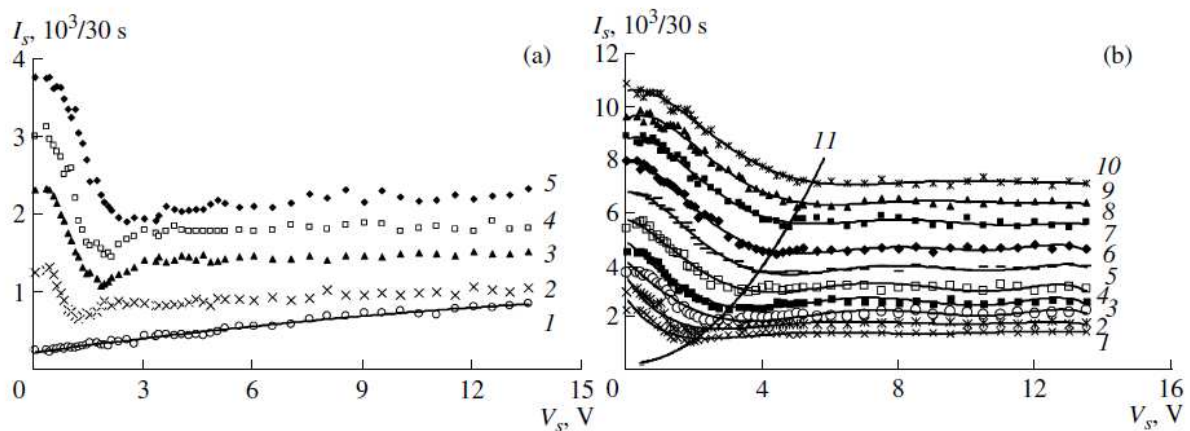


Figure 19. Diffraction intensity of the (440) reflection as a function of the US wave amplitude for different h , (a) (1) $h = 0$ (perfect crystal); (2) $1 \mu\text{m}$; (3) $3 \mu\text{m}$; (4) $5 \mu\text{m}$; (5) $7 \mu\text{m}$. (b) (1) $5 \mu\text{m}$; (2) $7 \mu\text{m}$; (3) $9 \mu\text{m}$; (4) $12 \mu\text{m}$; (5) $16 \mu\text{m}$; (6) $20 \mu\text{m}$; (7) $25 \mu\text{m}$; (8) $30 \mu\text{m}$; (9) $35 \mu\text{m}$; (10) $40 \mu\text{m}$; (11) displacement of the diffraction minimum along V_s as a function of h .

The simultaneous effect of both deformation types of a crystal lattice, static bending and dynamic atomic displacement in an US wave, on the neutron diffraction in the Laue geometry was taken into account in [14,46] where numerically (by the method of successive approximation) and, for separate cases, analytically by a modified Takagi-Taupin equation was solved. In [49], for this purpose Green's functions were used for Laue case. In the case of the Bragg geometry the mathematical task is substantially complicated because of specific boundary conditions and, as we know, has no analytical solutions up to now. The semi-phenomenological model explaining qualitatively the experimental results and allowing us to obtain quantitative characteristics in some cases is considered below in the framework of the dynamic scattering theory. The problem solution for the case of Laue diffraction in smoothly deformed crystals was described by us above and this model is also applied for the case of the Bragg geometry.

The role of US in a modified PPK model is the resonance suppression of adiabatic motion of tie points by analogy to Laue diffraction and schematically transition to the Bragg case can be done if to turn the Fig. 12 on 90° [23]. The relative change in the diffraction intensity η can be again written in the form:

$$\eta = (I_{ds} - I_{d0}) / I_{d0} = P^2 + M^2 - 1 = -2MP < 0 \quad (27)$$

$$\eta = (I_{ds} - I_{d0}) / I_{d0} = P^2 + M^2 - 1 = -F(B)MP < 0, \quad (28)$$

where $0 < F(B) < 2$ for the case $v_s > v_{res.}$.

One can see that Expr. 27,28 coincides closely with Expr. 18,19 for the Laue diffraction.

Then we obtain $(Hw)_{min}$, the position of the η minimum depending on the deformation gradient.

$$(Hw)_{min} = (\ln 2B)^{0.5} \quad (29)$$

The changes of η as a function of Hw are shown in Figs. 20a and 20b for comparison of the experimental data to the described model. Expressions (27-29) satisfactorily describe the experiment only for the case of small Hw and small B (large bending radii) ($Hw < 0.3$ and $h < 7 \mu\text{m}$). With an increase in both parameters these expressions do not correspond to the experimental data shown in Fig. 21b which are rather well described by the Bessel functions expanded in the alternating series.

Expressions (27-29) are valid for one-phonon processes of the energy exchange between the neutron and US phonon.

Using relation $Hw = cV$ and assuming $B = \alpha h$, Eq. (29) can be rewritten in the form

$$V_{smin} = \alpha_1 h^m \quad (30)$$

The graphs of the positions of minima η as a function of h are shown in Fig. 21 for the (220) and (440) reflections. The exponent m is 0.49 for the (220) reflection (curve 2) and 0.46 for the

(440) reflection (curve 1) and $\alpha_{1(440)}/\alpha_{1(220)} = 1.83$, which is rather close to the theoretical estimations of the exponent of 0.5 and ratio $H_{440}/H_{220} = 2$. The value of the deformation gradient B is easily determined from here.

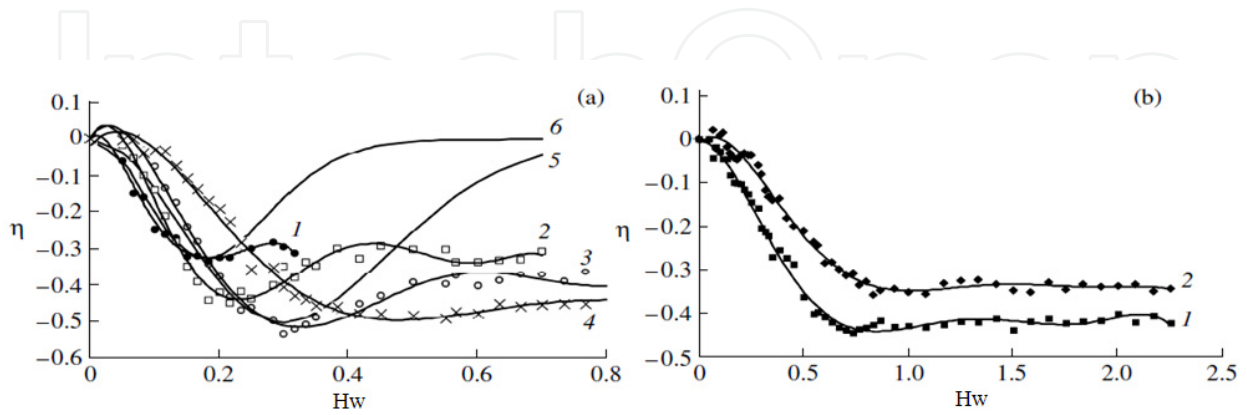


Figure 20. Relative changes in the diffraction intensity as a function of the US wave amplitude for different h : (a) (1) $h = 0.4 \mu\text{m}$; (2) $1 \mu\text{m}$; (3) $3 \mu\text{m}$; (4) $7 \mu\text{m}$; curve 5 corresponds to Eq. (5) for $F(B) = 2.0$, $F(B) = 1.3$ for curve 6. Solid curves 1–4 are fitting (Exprs.(27-29)) (b)1- $h = 9 \mu\text{m}$; 2- $h = 16 \mu\text{m}$

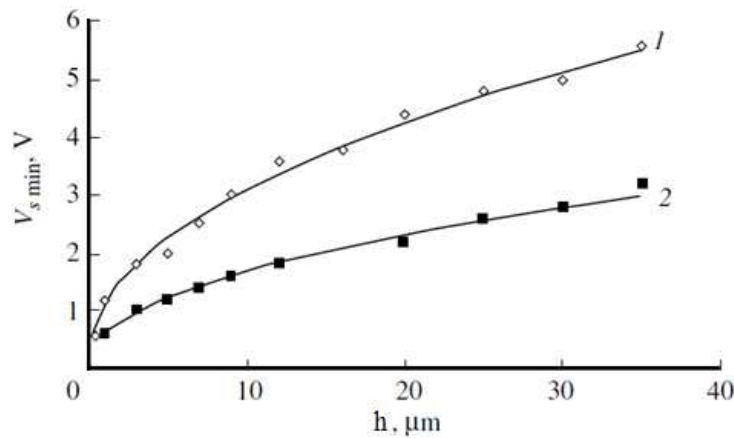


Figure 21. Shift of the minimum of $V_{s \text{ min}}$ for relative changes in the diffraction intensity η with an increase in the value of bending deflection h : 1: (1) for (220) reflection; (2) for (440) reflection.

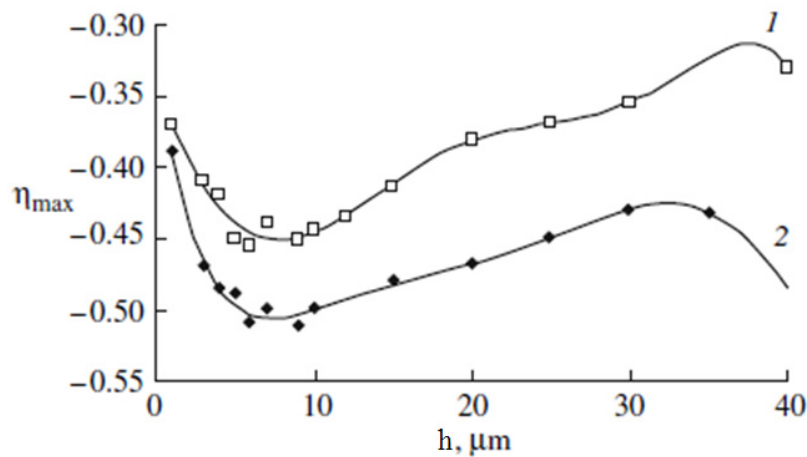


Figure 22. Dependence of the value of maximal dip of the relative diffraction intensity of neutrons η_{max} on the value of bending of a crystal: (1) for (220) reflection; (2) for (440) reflection. Solid curves are fitting obtained by an expansion of the Bessel function in a Taylor series.

As it follows from Eq. (29), the maximal dip of the relative deformation's intensity η_{max} shown in Fig. 22 is close to 0.5 for the (220) reflection and is reached for the bending radius $R = 200\text{--}600$ m. Thus, the PPK model modified for the case of ultrasound excitation satisfactorily describes some features of the neutron Bragg scattering from a bent silicon single crystal. The intensity dip of the Bragg diffraction is caused by the resonance transitions of the tie points between the sheets of dispersion surface related to the presence of ultrasound phonons. The position of the maxima depending on the investigated reflections and bending radius of a crystal is determined by the most probable single-phonon scattering of neutrons. With an increase in the US wave's amplitude and the value of crystal bending the role of less probable multi-phonon processes is enhanced, which results in the formation of a plateau in the curves of the voltage dependence of intensity on a piezoelectric transducer and bending radius.(Fig. 18).

5. Conclusion

For describing the diffraction in single perfect crystals the theory of dynamical neutron scattering has been employed. This approach considers the neutron wave pattern propagating in the periodic potential of an ideal lattice, and a variety of features is explained by this time, including an oscillating form for the distribution of the diffracted intensities within the Bormann fan in the case of Laue diffraction. One of the most important dynamical diffraction effects being the strongly limited intensity diffracted by an ideal crystal in Bragg's position. While, the interference effects disappear very quickly if the translation symmetry in a perfect crystal is violated due to any disturbance (static deformation strain, low-frequency sound excitations, etc.) and the Bragg-reflected intensity

increases. In our work it is shown that even a very sharp rising diffraction intensity at the center of Bormann's fan ($I_s / I_0 \geq 10$) can be described quantitatively using the dynamic diffraction model for the neutrons propagating in a thick crystal as spherical wave.

The PPK model modified for the case of ultrasound excitation satisfactorily describes some features of the neutron Bragg scattering from a bent silicon single crystal. The intensity dip of the Bragg diffraction is caused by the resonance transitions of the imaging points between the sheets of dispersion surface related to the presence of ultrasound phonons. The position of the maxima depending on the investigated reflection and bending radius of a crystal is determined by the most probable single-phonon scattering of neutrons. With an increase in the US wave's amplitude and the value of crystal bending the role of less probable multiphonon processes is enhanced, which results in the formation of a plateau in the curves of the voltage dependence of intensity on a piezoelectric transducer. These effects described phenomenological in the given work are not taken into consideration by the simple PPK model.

Author details

E. Raitman, V. Gavrilov and Ju. Ekmanis
Institute of Physical Energetics, Riga, Latvia

Acknowledgement

The authors thank Prof. V.A. Somenkov (Kurchatov's Center, Moscow, Russia) for unique Ge sample used in this work and Dr. A.Hoser for help in the measurements. The research at HZB BENSC (Germany) was supported by EU programme contract NM13 II-1523.

6. References

- [1] G. W. Fox, P. H. Carr, (1931) *Phys. Rev*, 37, 1622,
- [2] W.J.Spencer, and G.T.Pearman, (1970), *Adv.X-ray Analysis* 13,307,
- [3] T. F. Parkinson, M. W. Moyer, (1966)*Nature* 211, 400,
- [4] J.W.Knowles, (1956), *Acta Cryst.* 9, 61,
- [5] .D.Zippel, D.Kleinstuck, and G.E.R.Shulce, (1965)*Phys.Lett.*14, 174,
- [6] A.V.Kozlov, and A.I.Frank (2005) , *Phys.At.Nuclei* 68,7,1104,
- [7] J.Summhammer (1993)*Phys.RevA*47,556,
- [8] M.Moshinsky (1952) *Phys.Rev.* 88,625,
- [9] A. R. Mkrtychyan, M. A. Navasardian, R. G. Gabrielyan, and L. A. Kocharian, (1986) *Solid St.Comm.* 59(3), 147,
- [10] R. Hock, T. Vogt, J. Kulda, Z. Mursic, H. Fuess, A. Magerl, (1993) *Zeit. Phys. B* 90, 143,
- [11] A. Remhof, K.-D. Liß, A. Magerl, (1997) *NIM A*391, 485,

- [12] J.P. Guigay, P. Mikula, R. Hock, R. Baruchel, and A. Waintal, (1990) *Acta Cryst.* A46, 821,
- [13] E. Zolotoyabko, B. Sander, (1995) *Acta Cryst.*, A51, 163.
- [14] Iolin, E., Raitman, E., Kuvaldin, B., Gavrilov, and V. & Zolotoyabko, (1988) *E. Zh. Eksp. Teor. Fiz.* 94, 218,
- [15] S. D. LeRoux, R. Colella, and R. Bray, (1975) *Phys. Rev.Lett.*, 35(4), 230.
- [16] E.Iolin, and I.Entin, (1983) *Zh. Eksp. Teor. Fiz.*,85,1692,
- [17] V. L. Nosik, (1994) *Cryst. Rep.*, 39(4),526,
- [18] S. Kikuta, T. Takahashi, S. Nakatani, (1984) *Jap. Journ. Appl. Phys.*, 23(4), L193,
- [19] R. Tucoulou, I. A. Schelokov, D. V. Roshchupkin, M. Brunel, L. Ortega, and P. Cevallier, (1995) *Opt. Commun.* 118, 175-180,
- [20] K.-D. Liss, A. Magerl, R. Hock, A. Remhof, B. Waibel, (1997) *Europhys. Lett.*, 40(4), 369,
- [21] E.M.Iolin, L.L.Rusevich, M.Vrana *et. al* (1996) *Phys.Status Sol.(b)* 195, 21,
- [22] E.Iolin, E. Raitman, *et. al.* (1986) *Sov. Phys. JETP.* 66, 218.,
- [23] E.Raitman, V.Gavrilov *et. al.*, (2009) *Surf. Invest.* 6, 3,
- [24] A. Blagov, M. Kovalchuk, V. Kohn, (2006) *Crystallography* 51,1,
- [25] V.L.Aksenov, H.Fritzsche, V.Gavrilov, Yu.Nikitenko, V. Progladio, and E.Raitman, (2004) *Latv. Journ. Phys. Techn. Sci.*, N 6, 1,
- [26] Felber J., Gähler R., Rauch C., and Golub R. (1996) *Phys. Rev.*A53, 319,
- [27] P.Micula, P.Lucas, and J.Kulda, (1992) *Acta.cryst.* A48, 72 ,
- [28] E.Iolin, L.Rusevich, M.Vrana, P.Mikula, and P.Lukas, (1996) *phys.stat.sol.(b)*,195,21,
- [29] V.N.Gavrilov, E.V.Zolotoyabko, and E.M.Iolin (1990) *Hyperfine Intereactions* 58, 2427,
- [30] V.N.Gavrilov, E.V.Zolotoyabko, and E.M.Iolin, *J.Phys.* C21, 471, 1988
- [31] I.Entin (1977) *Sov.Phys.JETP Lett.*50, 269,
- [32] I.Entin, and I.Puchkova (1984) *Sov. Phys.Solid State*, 26,1995,
- [33] R.Kohler, W.Mohling, and H.Peibst (1974) *Phys.Stat. Solidi B*61,173,
- [34] S. Takagi, (1962) *Acta Crystallogr.* 15 1311,
- [35] D. Taupin, (1961) *Bull. Soc. Fr. Miner. Crist.* 84 51,
- [36] C.G.Shull *J. Appl.Cryst.* 6, 257, 1973
- [37] A.Leilinder, C.G.Shull, J.Arthur, and M.A.Horn, (1983) *Phys.Rev.* A28,487,
- [38] C.G.Shull (1968) *Phys.Rev.Lett.*, 21,1585,
- [39] H.J.mc Skimin (1950) *J.Acoustic.Soc.of Am.* 22, ,413,
- [40] Yu.G. Abov, N.O. Elyutin, et al. (2002), *Phys. At. Nucl.* 65 (11), 1933 ,
- [41] Kato, N. (1964) *J. Phys. Soc. Jpn.* 19,
- [42] B.Kuvaldin, (1991), Private Comm., Riga,
- [43] E. Iolin, B. Farago, E. Raitman, F. Mezei. (1998), *Physica B* 241-243, 1213,
- [44] R.Hock, T.Vogt, J.Kulda, Z.Mursic, H.Fuess, and A.Magerl, 1993 *Z.Phys.*B90, 143,
- [45] F.N. Chukhovskii, V.L.Nosik, & E. M. Iolin, (1993) *JTEP (Sov.)* 104, 2452,
- [46] Iolin E., Raitman, E., Gavrilov, V., & Rusevich, L.. (1995) *J. Phys. D.: Appl. Phys.*28, A281
- [47] Penning, P.(1966) *Philips Res. Rep.*, suppl.,5, 1

[48] N.Kato and Y.Ando (1966)J.Phys.Soc. Jpn. 21,964,

[49] E.A.Raitman, V.N.Gavrilov *et. al.* (2008), Latvian J. Phys.Tech. Sci., 2, 13,

IntechOpen

IntechOpen